CFD simulation of propeller noise

Takuya Tachikawa[1], Nobuhiro Hasuike[2], and Keita Fujiyama[3]

[1,2]Nakashima Propeller Co., Ltd., Okayama/Japan, web page: http://www.nakashima.co.jp/
[3]Software Cradle Co., Ltd., Osaka/Japan, web page: https://www.cradle-cfd.com/
E-mail: [1]t-tachikawa@nakashima.co.jp,[2]nobuhiro@nakashima.co.jp, [3]fujiyama@cradle.co.jp

1 Introduction

Propeller cavitation causes under water radiated noise. Low frequency tonal noise is mainly related to the volume variation of the sheet cavitation which is the formation of unity of the cavitation bubbles. On the other hand, the high frequency noise is related to the dynamics of the micro cavity collapse and its rebound after the division. The bubble radius, the ambient pressure and the initial gas contents are dominant factors of the bubble dynamics and its resulted sound pressure.
Recently developed "Multi-process cavitation model" (Tsuda et al.[1], 2015) is considering the basic bubble dynamics like as bubble expansion/shrinkage with bubble-bubble interaction, evaporation/condensation, inception/collapse, coalescence and break-up. "Multi-process cavitation model" provides the distribution of the number density and the bubble radius analytically. By using these information, the radiated sound pressure by each single bubble can be estimated by Rayleigh-Plesset equation with compressibility. In this study, combination of "Multi-process cavitation model" and simple bubble dynamics was discussed.

2 Multi-process cavitation model

The "Multi-process cavitation model" (Tsuda et al.[1], 2015) is constructed based on the moment method. "*i*th moment *Mi* is defined using the size distribution function *f(R, t)*.

$$\boldsymbol{M_i = \int R^i f(R,t)\, dR} \qquad (1)$$

Taking the time derivative for the quantity *Mi*, following relationship is derived.

$$\boldsymbol{\frac{DM_i}{Dt} = iG(\bar{R})M_{i-1} + S_{p,i}(for\ i = 0,1,2,3)} \qquad (2)$$

Where, $f(R,t)$ is size distribution function. $\bar{R}$ is mean radius of bubbles defined as M_1/M_0. $G(\bar{R})$ is expansion and shrinkage speed. $S_{p,i}$ reflects the change of the number of bubbles, which occurs with inception/collapse and break up/coalescence.

$$\boldsymbol{G(\bar{R}) = \frac{d}{dt}\left(\frac{M_1}{M_0}\right)} \qquad (3)$$

$$\boldsymbol{\bar{R} = \frac{M_1}{M_0}} \qquad (4)$$

R_c is critical size. J_s is inception and collapse rate. S_b and S_c are break-up and coalescence rate respectively. $\dot{m}_v$ is evaporation and condensation flux.

Expansion/ Shrinkage — Inception/ Collapse — Coalescence/ Break-up

$$\boldsymbol{\frac{DM_0}{Dt} = J_s + S_b - S_c} \qquad (5)$$

$$\boldsymbol{\frac{DM_1}{Dt} = G(\bar{R})M_0 + R_c J_s + \bar{R}(S_b - S_c)} \qquad (6)$$

$$\boldsymbol{\frac{DM_2}{Dt} = 2G(\bar{R})M_1 + R_c^2 J_s + \overline{R^2}(S_b - S_c)} \qquad (7)$$

$$\boldsymbol{\frac{DM_3}{Dt} = 3G(\bar{R})M_2 + R_c^3 J_s + \overline{R^3}(S_b - S_c)} \qquad (8)$$

$$\boldsymbol{\frac{D(\rho_g M_3)}{Dt} \approx \dot{m}_v M_2 M_3 + \rho_g \frac{DM_3}{Dt}} \qquad (9)$$

Evaporation/ Condensation

Void fraction ϕ and Quality Y are derived as followings;

$$\phi = \frac{(4\pi/3)\mathbf{M_3}}{\mathbf{1} + (4\pi/3)\mathbf{M_3}} \quad (10)$$

$$\mathbf{Y} = \frac{(4\pi/3)\rho_g M_3}{\rho_l + (4\pi/3)\rho_g M_3} \quad (11)$$

3 Numerical simulation of cavitation performance

"Multi-process cavitation model" was implemented to commercial solver Software Cradle SC/Flow 2020, which is the navier-stokes solver based on a finite volume method. The coalescence and break-up term were neglected in this study. To simulate the two-phase cavitating flow, the single fluid approach was used. In addition, the mixture density was treated as a compressible flow by using barotropic relation. SST k-ω model was used. In practical view of simulation, CFD simulation neglected the second order derivative of Rayleigh-Plesset equation.

Numerical grids

Seiun-Maru HSP II propeller[2,3] was selected for this study(See Fig. 1). Principal particulars of the ship and the propeller and operating condition are shown in Table 1. Simulation was conducted in model scale. The computational domain was composed of the inner rotational part including the propeller and the outer stationary part including hull. Unsteady propeller simulation in the wake uses the sliding mesh methodology. The numerical mesh was an unstructured grid. Basic meshes were polyhedral and prismatic cells were applied to near the blade surface for resolving the boundary layer. The first layer thickness of the prism layer was set to a non-dimensional wall distance for a wall-bounded flow (y^+ in short) =50. The second order accuracy of the convective term was adapted. The region was the same size as the large cavitation tunnel in NMRI (See Fig. 2). In the experiments, auxiliary equipment called Flow Liner was installed to simulate the full scale ship wake distribution.

The thrust coefficient k_T was adjusted to 0.201 as predefined value by changing the inflow speed.

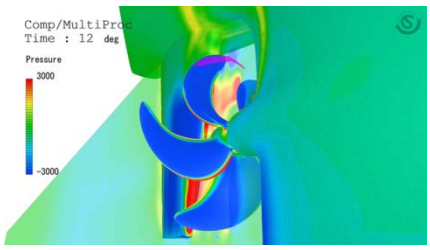

Figure 1: Seiun-Maru HSP II propeller

Table 1 Principal particulars[2,3]

			Ship	Model
Ship length	L_{wl}	m	109	6.687
Propeller diameter	D_p	m	3.6	0.22
Thurst coefficient	k_T	-		0.201
Cavitation number	σ_n	-		2.99
Shaft speed	n	rps	2.72	17.5

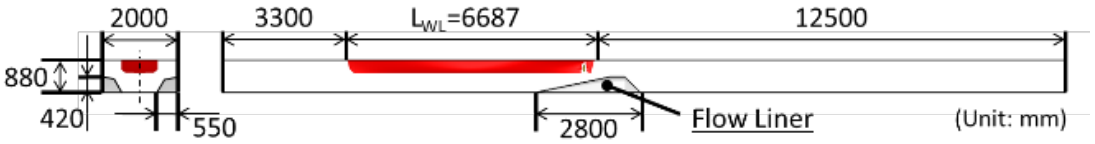

Figure 2: Computational domain

Pressure pulse simulation

The tonal noise up to 100Hz is related with the pressure pulse caused by the whole sheet cavitation dynamics. Therefore, the estimation accuracy of pressure pulse of blade frequency component is important for the prediction of the low frequency noise. The first and the second order blade frequency components of pressure amplitude were compared in Fig. 3. For the first order blade frequency components, "Multi-process cavitation model" (MP) showed better agreement in

comparison with Full cavitation model (FCM)[4]. On the other hand, both cavitation models underestimated the second order blade frequency components.

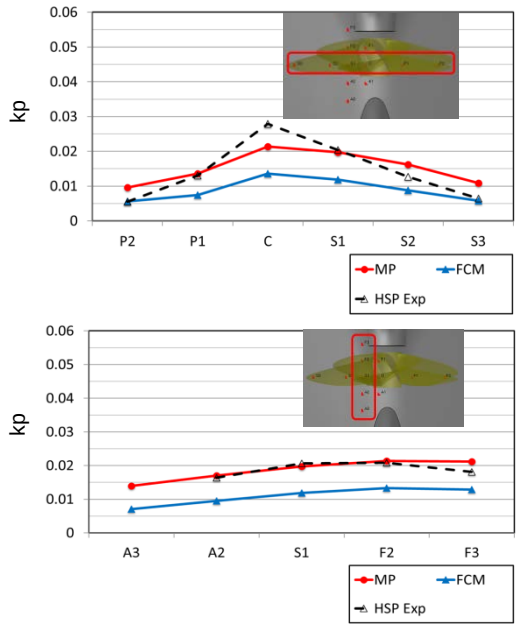

Figure 3: Comparison of the first order component of pressure pulse

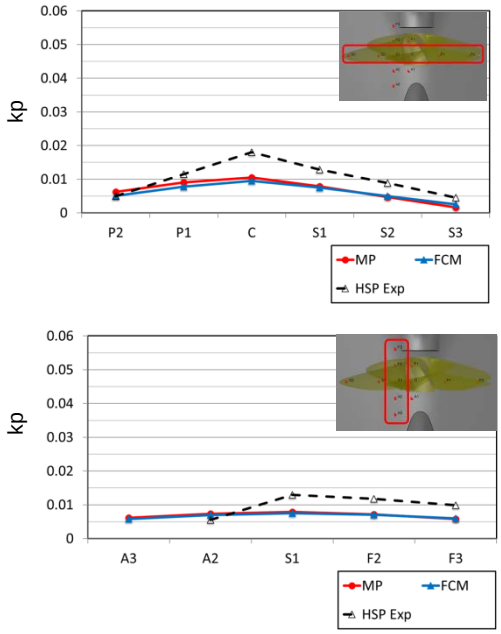

Figure 4: Comparison of the second order component of pressure pulse

Cavitation pattern and distribution of cavitation bubbles

In order to simulate the cavitation noise, estimation accuracy of cavitation volume is important. The cavitation pattern simulated by "Multi-process cavitation model" was compared with experimental results. Fig. 5 shows the comparisons of the cavitation pattern between the experiment and the isosurface of 10% void fraction from the calculations. Calculation result showed good agreement with model experiment.

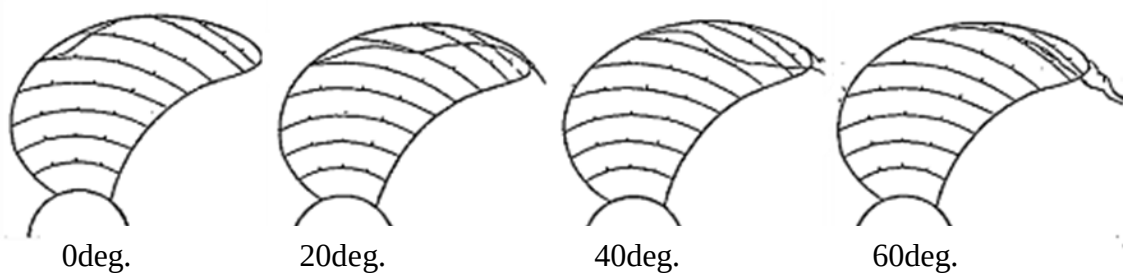

Figure 5(a): Cavitation patterns(Experiment)

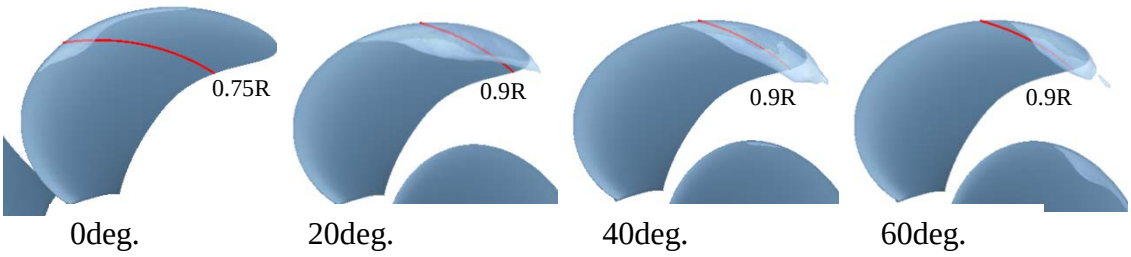

Figure 5(b): Cavitation patterns(MP)

Bubble distribution

Simulated number and radius of bubbles at 45deg. are shown in Fig. 6(a) and (b), which was the blade position with maximum cavity size. The bubble radius increased with expansion of the sheet cavitation. The bubble radius decreased with whole cavity shrinkage. The number of cavitation nuclei

and bubble radius were smaller near the surface of the sheet cavitation. The bubble radius at 0.85R was mainly from 2.5 to 3.0mm. Smaller bubbles are located near the sheet cavity surface. The bubble radius at 0.90R was from 2.5 to 4.0mm. The bubble radius at 0.95R and 0.975R were mainly from 3.5 to 4.5mm.The bubbles in the sheet cavitation grew and moved from leading edge to trailing edge. The bubbles at 0.95R grew more in comparison with those at 0.85R by the lower pressure at the leading edge. On the other hand, the cavitation at 0.975R included the sheet cavitation and the tip vortex cavitation. The tip vortex cavitation was generated near the leading edge and stably maintained along the tip vortex core. The tip vortex cavitation including large bubbles seemed to play an very important role for its high frequency noise, because the large bubbles generates the large sound pressure of the shock wave impulse.

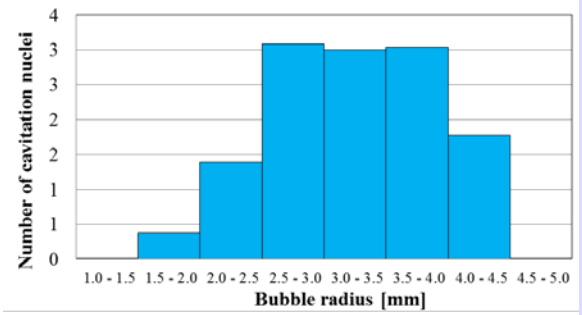

Figure 6(a): Distribution of the number and the radius of the bubbles at 45deg. position

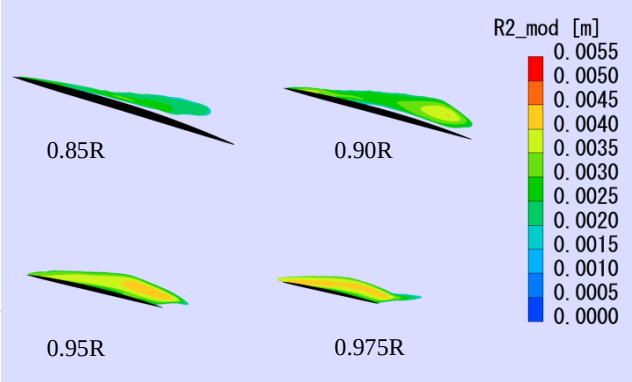

Figure 6(b): Distribution of the bubble radius

Noise prediction

In this study, several noise simulation approaches were studied as practical design tools.

(a) Direct simulation of pressure pulse at receiver position

(b) Brown formula[5](1977)

Brown's formula assumes the relation between cavitation area and the high frequency noise. As estimation of cavitation area by calculation or model experiment is consistent and visible, this kind of approach is attractive for daily use.

$$SPL_{src} = K + \log_{10}\left(BD_p{}^4 n^3 f^{-2}\right) + \log_{10}(A_c/A_D) \qquad (12)$$

Where, SPL_{src} $[dB\ re\ 1\mu Pa/\sqrt{Hz}\ at\ 1m]$ is the sound source level. K is an empirical constant which is used as 163 at the standard propeller case and B is the number of the blades. A_c [m^2] is the area of cavity on the blade, and [m^2] is the area of the blade. A_c/A_D was 0.11, which was decided by referring maximum A_c/A_D from the CFD results with consideration of safety side.

(c) Single bubble dynamics equation(Tomita and Shima et al.[6], 1977)

Single bubble dynamics was solved by Tomita and Shima method which includes the compressibility (Eq. (13)-(15)). The sound pressure by one bubble p_a is derived by Eq. (16). Total sound pressure level was derived by summation of each bubble. This approach was suggested by Kamiirisa et al.[7](2005) and Ando et al.[8](2018). The merit of using bubble dynamics was that time history of the bubble radius and the impulse pressure was easily treated without the problem of the spatial mesh density, although the coupling of the flow field solved by the CFD and the bubble dynamics is one way coupling.

This approach needed an assumption of initial bubble radius and number of the cavitation nuclei. "Multi-process cavitation model" was expected to give theoretical number of the cavitation nuclei and the bubble radius. In this study, the initial radius and the number of bubbles were referred from the number and the radius distribution at 45deg. simulated by "Multi-process cavitation model", which was the blade position with maximum cavity. By this way, the initial dR/dt for Lunge Kutta calculation was approximately treated as zero.

$$R\ddot{R}\left[1-(1+\varepsilon)\frac{\dot{R}}{C_\infty}+\left(-1+\frac{7}{2}\varepsilon-\frac{\varepsilon^2}{5}\right)\frac{\dot{R}^2}{{C_\infty}^2}\right]$$
$$+\frac{3}{2}\dot{R}^2\left[\frac{4-\varepsilon}{3}-\frac{4}{3}\frac{\dot{R}}{C_\infty}+\left(\frac{-4}{3}+4\varepsilon-\frac{43}{30}\varepsilon^2+\frac{\varepsilon^3}{6}\right)\frac{\dot{R}^2}{{C_\infty}^2}\right]$$
$$+\frac{1}{\varepsilon\rho_\infty}\left[p_\infty-p_{2_{r=R}}-\frac{R\dot{p}_{1_{r=R}}}{C_\infty}\right.$$
$$\left.+\frac{1}{{C_\infty}^2}\left\{(1+\varepsilon)R\dot{R}\dot{p}_{1_{r=R}}+\left(p_\infty-p_{1_{r=R}}\right)\left[\left(-2+\frac{7}{2}\varepsilon-\varepsilon^2\right)\dot{R}^2+\frac{3}{2}\frac{p_\infty-p_{1_{r=R}}}{\rho_\infty}\right]\right\}\right]$$
$$=0 \tag{13}$$

$$p_{1_{r=R}}=\frac{-2\sigma}{R}+p_0\left(\frac{R_0}{R}\right)^{3\gamma}+\rho_g\varepsilon\dot{R}^2-\varepsilon\frac{4\mu\dot{R}}{R} \tag{14}$$

$$p_{2_{r=R}}=p_{1_{r=R}}+\frac{\varepsilon}{{C_\infty}^2}\left(\frac{4\mu}{3}+\zeta\right)\left\{\frac{3}{2}\varepsilon(1-\varepsilon)\frac{\dot{R}^3}{R}-\frac{\dot{p}_{1_{r=R}}}{\varepsilon\rho_\infty}+(1-\varepsilon)\frac{\left(p_\infty-p_{1_{r=R}}\right)\dot{R}}{\varepsilon\rho_\infty R}\right\} \tag{15}$$

$$p_a=\frac{\rho_l}{4\pi r}\frac{d^2V}{dt^2} \tag{16}$$

Where, C_∞ is the velocity of the sound in the liquid at infinity. γ is the ratio of the specific heats of gas. ζ is the bulk viscosity of the liquid. μ is the viscosity of the liquid. σ is the surface tension of the liquid. R and R_0 are the radius and the initial radius of the bubble. V is the volume of the bubble. p_0 is the initial gas pressure inside the bubble. p_∞ is the pressure in the liquid at infinity. p_a is the sound pressure at radial distance r from the bubble center. The pressure in the liquid at the bubble wall $p_{ir=R}$ can be written in Eq. (14) and Eq. (15) as the ith approximation. ρ is the density where the subscripts of "g" and "l" denote the gas and the liquid respectively. ε is the ratio defined with the gas density and density at infinity($\varepsilon=1-\rho_g/\rho_\infty$).

Fig. 7 shows the sound receiver positions. The tonal noise is related to the dynamics of the sheet cavitation which is the unity of the bubbles. In this case, the tonal noise can be scaled as the monopole (See Eq. (18)). On the other hand, the higher frequency noise can be treated as the shock wave impulse and scaled by Levkovskii[9](1968) Eq. (19). Where, the subscripts of "m" and "s" denote model and full scale, respectively, and $V=nD_p$.

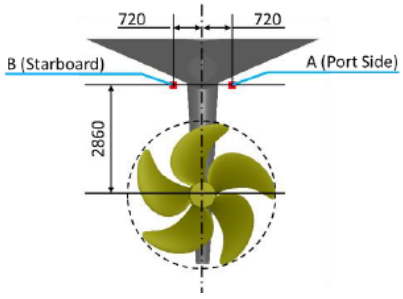

$$\lambda=D_{ps}/D_{pm} \tag{16}$$

$$\frac{f_s}{f_m}=\frac{n_s}{n_m} \tag{17}$$

$$SPL_s-SPL_m=10\log_{10}\left[\lambda^6\cdot\left(\frac{n_s}{n_m}\right)^4\cdot\left(\frac{{r_m}^2}{r_s}\right)\right] \tag{18}$$

$$SPL_s-SPL_m=10\log_{10}\left[\lambda^5\cdot\left(\frac{n_s}{n_m}\right)^2\cdot\left(\frac{{r_m}^2}{r_s}\right)\right] \tag{19}$$

Figure 7: Sound receiver position

Fig. 8(a) and (b) show the computational and experimental results of the sound pressure level on the sound receiver position at B (starboard side). Narrow band estimation results showed clear blade frequency components as tonal noise.

Direct simulation of the pressure pulse at the receiver position showed good agreement with the experimental result around the first to the fourth blade passing frequency range, which was from 10Hz to 100Hz in this case. However, the prediction did not agree with the experimental results over hundreds Hz. CFD simulation neglected the second order derivative of Rayleigh-Plesset equation. The numerical mesh and time step seemed to be still coarse for the collapsing of bubble. These seemed to bring the limitation for the higher frequency noise estimation. The results by the Brown's method showed good agreement between middle hundreds Hz and middle thousands Hz region. Tomita-Shima method combined with the information from "Multi-process cavitation model" showed also good agreement between middle hundreds Hz and middle thousands Hz region. Direct simulation

of pressure pulse at receiver position well predicts the noise level at low frequency.

For higher frequency noise prediction, the Brown's formulae based on the cavitation area derived from CFD are practical as design tool. Tomita-Shima method based on the number and the radius of the bubbles derived by "Multi-process model" seems to be also the good measure.

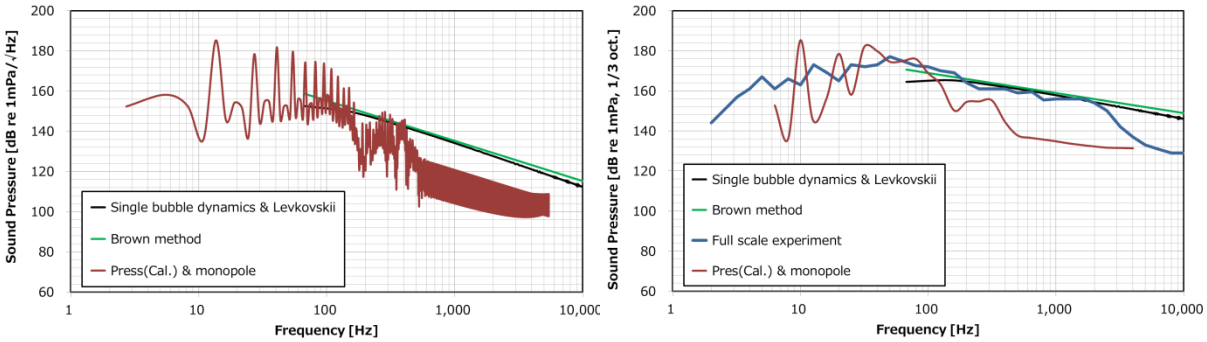

(a) Narrow band (b) 1/3 oct. band

Figure 8: Sound pressure estimation resutlt

4 CONCLUTIONS

In this study, newly developed "Multi-process cavitation model" was adopted for the unsteady cavitation simulation.

1) The unsteady cavitation pattern behind ship condition was well reproduced by the "Multi-process cavitation model".
2) "Multi-process cavitation model" gave distribution of number of cavitation nuclei and bubble radius which was related to higher frequency noise.
3) Direct noise predictions showed good agreement up to 5th blade passing frequency with monopole scaling method. It seems to be difficult to predict the accurate noise level by the direct CFD calculation at over hundreds frequency range noise.
4) Brown's empirical formula or Tomita-Shima method in combination with "Multi process cavitation model" showed good capability for practical estimation at over hundreds frequency range noise.

5 REFERENCES

[1] Tsuda, S. and Watanabe, S., "Application of Multi-Process Cavitation Model for Cavitating Flow in Cold Water and in Liquid Nitrogen around a Hydrofoil", Proc. ASME/JSME/KSME 2015 Joint Fluids Engineering Conf., Paper No. AJKFluids2015-05532.

[2] Gindroz, B.,Hoshino, T. & Pylkkanen, V., "Propeller RANS/Panel Method Workshop, 22nd ITTC Propulsion Committee Propeller RANS/Panel Method Workshop", Grenoble, Apr.1998.

[3] Hoshino,T. , "Experimental Data For Unsteady Panel Calculations And Comparison (Seiun-Maru HSP)", Proceedings of Propeller RANS/Panel Method Workshop, 22nd ITTC Propulsion Committee, Grenoble, Apr.1998.

[4]Singhal A. K., et al., "Mathematical basis and validation of the full cavitation model", Journal of Fluids Eng. 124(3), pp.617-624, 2002

[5] Brown. N.A.,"Cavitation noise problems and solutions", Proc. International Symposium on Shipboard Acoustics, pp.21-38, 1977

[6] Tomita, Y. and Shima, A., "On the Behavior of a Spherical Bubble and the Impulse Pressure in a Viscous Compressible Liquid", Bulletin of the JSME, Vol. 20, No. 149, 1977

[7] Kamiirisa et al., "Development of Prediction Method for Ship Underwater Noise by Bubble Dynamics", Mitsui Engineering & Shipbuilding Co Technical Review No.185, 2005

[8] Ando, S., Kimura, K., Segawa, K., Yamamoto, K., "Study on the Hybrid Method of CFD and Bubble Dynamics for Marine Propeller Cavitation Noise Prediction", Proceedings of the 10th International Symposium on Cavitation (CAV2018), 2018

[9] Levkovskii, Y.L.,"Modelling of cavitation noise", Soviet Physics-Acoustics 13, pp.337–339, 1968

[10] Fujiyama K., "Numerical Simulation of Ship Hull Pressure Fluctuation Induced by Cavitation on Propeller with Capturing the Tip Vortex", Fourth International Symposium on Marine Propulsors SMP'15, 2015